

See discussions, stats, and author profiles for this publication at: <https://www.researchgate.net/publication/45581906>

Tunable Band Gap in Hydrogenated Quasi-Free-Standing Graphene

ARTICLE *in* NANO LETTERS · SEPTEMBER 2010

Impact Factor: 13.59 · DOI: 10.1021/nl101066m · Source: PubMed

CITATIONS

157

READS

213

14 AUTHORS, INCLUDING:



Danny Haberer

University of California, Berkeley

23 PUBLICATIONS 684 CITATIONS

[SEE PROFILE](#)



Denis V Vyalikh

Technische Universität Dresden

210 PUBLICATIONS 3,096 CITATIONS

[SEE PROFILE](#)



Jörg H. Fink

Leibniz Institute for Solid State and Materi...

550 PUBLICATIONS 14,832 CITATIONS

[SEE PROFILE](#)



Stefano Simonucci

University of Camerino

47 PUBLICATIONS 594 CITATIONS

[SEE PROFILE](#)

Tunable Band Gap in Hydrogenated Quasi-Free-Standing Graphene

D. Haberer,[†] D. V. Vyalikh,[‡] S. Taioli,^{§,||} B. Dora,[⊥] M. Farjam,[#] J. Fink,^{†,▽} D. Marchenko,[▽] T. Pichler,[○] K. Ziegler,[◆] S. Simonucci,[¶] M. S. Dresselhaus,⁺ M. Knupfer,[†] B. Büchner,[†] and A. Grüneis*,^{†,○}

[†]IFW Dresden, P.O. Box 270116, D-01117 Dresden, Germany, [‡]Institut für Festkörperphysik, TU Dresden, Mommsenstrasse 13, D-01069 Dresden, Germany, [§]Interdisciplinary Laboratory for Computational Science (LISC), FBK-CMM and University of Trento, via Sommarive 18, I-38123 Trento, Italy, ^{||}Department of Physics, University of Trento, Via Sommarive 14, I-38100, Trento, Italy, [⊥]Department of Physics, Budapest University of Technology and Economics, Budapest, Hungary, [#]Institute for Research in Fundamental Sciences (IPM), P.O. Box 19395-5531, Tehran, Iran, [▽]Helmholtz-Zentrum Berlin für Materialien und Energie, Elektronenspeicherring BESSY II, Albert-Einstein-Strasse 15, D-12489 Berlin, Germany, [○]Faculty of Physics, University of Vienna, Strudlhofgasse 4, 1090 Wien, Austria, [◆]Institut für Physik, Universität Augsburg, D-86135 Augsburg, Germany, [¶]Department of Physics, University of Camerino, via Madonna delle Carceri 9, 62032 Camerino, Italy, and ⁺Department of Physics and Department of Electrical Engineering and Computer Science, Massachusetts Institute of Technology, Cambridge, Massachusetts 02139-4307

ABSTRACT We show by angle-resolved photoemission spectroscopy that a tunable gap in quasi-free-standing monolayer graphene on Au can be induced by hydrogenation. The size of the gap can be controlled via hydrogen loading and reaches ~ 1.0 eV for a hydrogen coverage of 8 %. The local rehybridization from sp^2 to sp^3 in the chemical bonding is observed by X-ray photoelectron spectroscopy and X-ray absorption and allows for a determination of the amount of chemisorbed hydrogen. The hydrogen induced gap formation is completely reversible by annealing without damaging the graphene. Calculations of the hydrogen loading dependent core level binding energies and the spectral function of graphene are in excellent agreement with photoemission experiments. Hydrogenation of graphene gives access to tunable electronic and optical properties and thereby provides a model system to study hydrogen storage in carbon materials.

KEYWORDS Graphene, hydrogenation, photoemission, X-ray absorption, hydrogen storage

The discovery of 2D graphene has led to a dramatic increase in research effort due to its remarkable physical properties.^{1,2} Graphene is a zero gap semiconductor with a linear energy band dispersion around the Fermi energy (E_F), so that the charge carriers mimic massless Dirac fermions.^{1,2} This allows one to address basic questions of quantum electrodynamics in a benchtop experiment.^{3,4} Nevertheless, the application of graphene in semiconductor devices requires a band gap in order to switch the conductivity between an on and off state. Physical and chemical approaches for opening a gap are under discussion. First, size quantization of about 1 nm induces band gaps of ~ 1 eV in graphene nanoribbons,^{5–7} nanotubes,⁸ and quantum dots.⁹ However, in the case of nanotubes, the preparation of samples with Ohmic contacts is still challenging. Similarly, in the case of nanoribbons, the electronic properties are determined by the edges,¹⁰ rendering this approach technologically very demanding. An alternative strategy is the chemical functionalization of graphene which induces band

gaps and can even be reversed.^{11–16} This approach was already successfully demonstrated before the discovery of graphene. For example, in hydrogenated amorphous carbon (a-C:H)¹⁷ an optical gap has been observed which increases with the hydrogen content.^{18,19} Fully hydrogenated graphene, also referred to as graphane, has been suggested recently as an insulator with a band gap of 3.5 eV²⁰ and doped graphane as a possible high- T_C superconductor.²¹ For partially hydrogenated graphene, Duplock et al. reported the appearance of a substantial band gap of 1.25 eV accompanied by a spin-polarized midgap state.²² With transport measurements, a metal to insulator transition (MIT) was observed after cleaved graphene on SiO_x was exposed to atomic hydrogen.²³ Much less is known about the band structure and the nature of the MIT. Furthermore, the amount of applied hydrogen could not be directly accessed by transport measurements. Hydrogenated graphene on SiC was investigated with angle-resolved photoemission spectroscopy (ARPES), suggesting an electron localization as the mechanism responsible for the MIT.²⁴ The transition itself was already observed at H coverages of ~ 0.1 %. However, graphene on SiC is intrinsically heavily electron doped (E_F is ~ 0.5 eV above the Dirac point) and as such is not the

* To whom correspondence should be addressed, alexander.grueneis@univie.ac.at.

Received for review: 03/26/2010

Published on Web: 08/09/2010

model system to be compared to the transport experiments on cleaved graphene. Similarly, scanning tunneling measurements of hydrogenated epitaxial graphene on an Ir substrate indicated graphene quantum dot formation and therefore a band gap opening that is determined by the quantum dot size.²⁵ In the above case, the strong interaction of graphene to the Ir and the patterned hydrogen chemisorption prevents a tunability of the electronic band gap. These profound limitations call for a different system from graphene on Ir and on SiC for studying hydrogenation.

In this Letter we demonstrate a tunable band gap in hydrogenated quasi-free-standing graphene on Au (E_F is at the Dirac point). The size of the gap depends exclusively on the H/C ratio and obtainable band gaps of up to 1 eV make this approach extremely appealing for applications in nanoelectronics and optics. The hydrogen induced gap formation is also fully reversible by modest annealing without damaging the graphene. Furthermore, both, the graphene on SiO_x and on Au have an identical doping level and a very similar electron energy band structure. Therefore hydrogenated quasi-free-standing graphene provides important input for understanding the transport experiments of hydrogenated graphene on SiO_x .

Experimental and Theoretical Methods. Pristine graphene samples were prepared under ultrahigh vacuum conditions by chemical vapor deposition on Ni(111) films.^{26,27} Hereafter 1 monolayer (ML) of Au was deposited on graphene and intercalated into the graphene/Ni interface by annealing.²⁸ This procedure liberates graphene from the strong substrate interaction rendering it quasi-free-standing. Hydrogenation of graphene/Au was performed by exposing graphene to a beam of atomic H that was produced by cracking H_2 at 2800 K in a W capillary at 2×10^{-9} mbar for 10–100 s. X-ray photoemission spectroscopy (XPS) of the C 1s core level and near edge X-ray absorption spectroscopy (NEXAFS) at the K-edge of carbon were performed to study the changes in the chemical bonding of graphene for each of the functionalization steps. These measurements were carried out at BESSY II using the German–Russian beamline and a SPECS Phoibos 150 analyzer. XPS was performed at a photon energy of 380 eV. ARPES was performed using a photoemission spectrometer equipped with a Scienta SES-200 hemispherical electron-energy analyzer, a high-flux He-resonance lamp (Gammadata VUV-5010) in combination with a grating monochromator. All valence PE spectra were acquired at a photon energy of $h\nu = 40.8$ eV (He^{II}) with an angular resolution of 0.3° and a total system energy resolution of 50 meV. All measurements were performed at room temperature. Calculations of the structural relaxation have been performed using the Vienna ab initio simulation package (VASP) and the pseudopotential implementation of ab initio total energy density functional theory. The C 1s line positions for as-grown graphene on Ni as well as with an Au ML intercalated in between the graphene/Ni interface and the hydrogenated graphene were calculated using

SURPRISES.^{29,30} The details of these calculations are given in the Supporting Information. The π band energy dispersion was described using simple nearest-neighbor as well as third nearest-neighbor tight-binding (3NN TB) parametrizations, which were then used to calculate changes in the electronic scattering rate upon H chemisorption within the relaxation-time approximation. Calculations of graphene's spectral function $A(E, k)$ for different H/C ratios were performed using a modified random gap model^{31–33} with the condition that if H is bound to a given lattice site, all of the three neighboring sites do not bond to H. As a result, a binary distribution was generated, i.e., a lattice site was either influenced by a strong local potential or not, while the above constraint ensured that the potential disorder is translated to random gap disorder. For a given lattice size, $A(E, k)$ was obtained after averaging over $\sim 10^4$ gap configurations. We provide more details and additional calculated results in the Supporting Information.

Results. Core-Level Spectroscopy and X-ray Absorption. Figure 1a illustrates the Au intercalation and hydrogenation procedure. Hydrogen induces a local sp^3 bonding thereby breaking double bonds to the neighboring carbon atoms. Atoms C1–C3 denote the chemical environments of unhydrogenated carbons, C atoms next to an sp^3 site, and C atoms in an sp^3 environment, respectively. In Figure 1b we show the C 1s core-level spectra of graphene. The line shapes depend sensitively on the chemical bonding of the C atoms to the Ni and Au substrate and the amount of hydrogenation. The binding energies and hydrogen coverage are determined with a Doniach Sunjic line shape analysis.³⁴ The initial C 1s peak for graphene on Ni is gradually disappearing as Au intercalation proceeds and a second C 1s peak emerges at 500 meV lower binding energy (we call this peak C1). Both peaks are visible for intercalation of 0.5 ML Au. After intercalation of 1 ML Au, only the lower binding energy peak remains, which indicates a substantially reduced bonding of graphene to the substrate. Following the hydrogenation we observe a dramatic change in the C 1s line shape. From the line shape analysis, we obtain two new peaks with locations at ~ 500 meV lower and higher (C2 and C3) binding energies than the C1 peak binding energy (which corresponds to the unhydrogenated C on Au). We assign the C2 peak to a shift in binding energy felt by a C 1s electron next to a hydrogenated carbon atom. The C3 peak can be identified with sp^3 bonded C atoms that form an out-of-plane C–H bond. This finding is in accordance with the reported results for hydrogenated SWCNTs and graphite.^{35,36} These works have shown that a shoulder at higher binding energy appears upon hydrogenation and that it can be attributed to the C 1s signal of the C–H bond. By comparing the relative peak areas of the C 1s components from the sp^2 and sp^3 carbon species, we obtain a maximum hydrogen coverage of about 25%, which is comparable to previously reported hydrogen coverages for SWNTs and graphite.^{35,37,36} Finally, we completely removed the hydrogen stored on

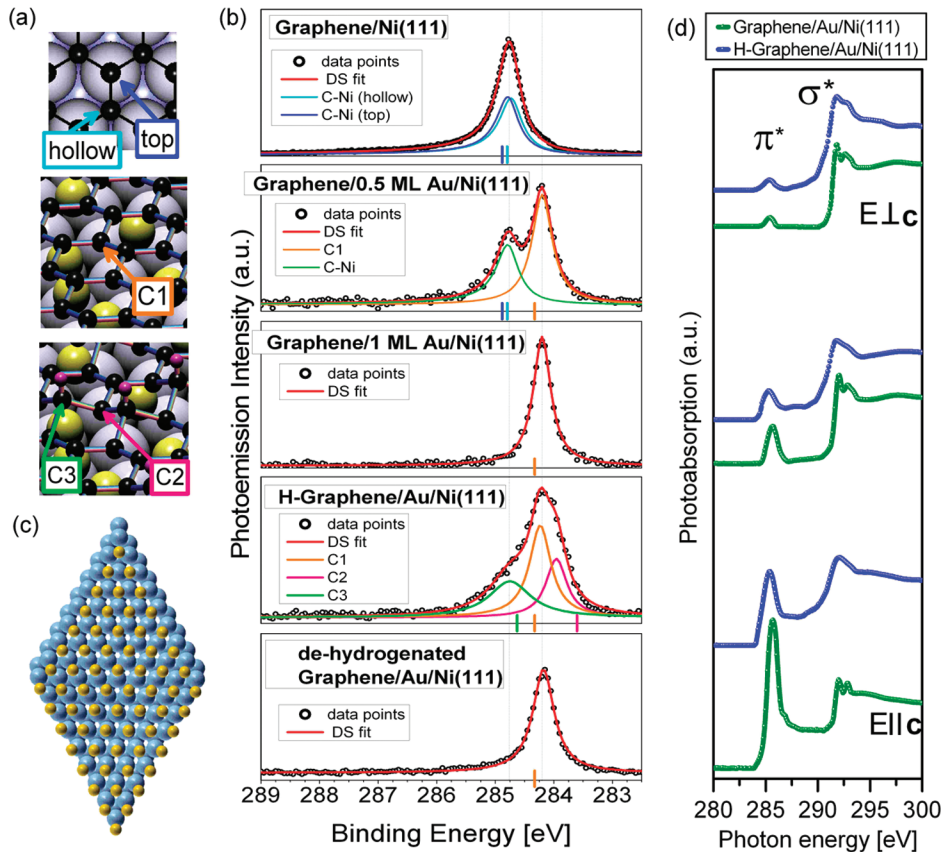


FIGURE 1. (a) Sketch of the functionalization procedure. From top to bottom: graphene on Ni(111), Au intercalated between the graphene/Ni interface, and hydrogenated graphene on Au. The hydrogen atoms are marked in violet. C1 and C2–C3 indicate chemical environments for graphene/Au and hydrogenated graphene, respectively. (b) C 1s core level spectra of graphene on Ni and on Au (0.5 and 1 ML of Au) and fully hydrogenated graphene. The bottom panel depicts graphene's C 1s level after dehydrogenation. All C 1s features were fitted with Doniach–Sunjic (DS) lineshapes with components for graphene/Ni (top and hollow sites), graphene/Au (C1) and hydrogenated graphene (C2–C3). The vertical lines on the energy axis correspond to the calculated C 1s energies of these components (the same color code applies). From the integrated area of the C–H component, we estimate a ~25% hydrogen load. (c) The optimized superstructure of one monolayer Au (8 × 8) on a Ni(111) surface (9 × 9). (d) X-ray absorption of pristine and hydrogenated graphene on Au for grazing incidence (bottom), ~45° (middle), and normal incidence (top). E and c denote the electric field vector and the sample surface normal vector, respectively.

graphene by heating the sample to ~600 K as is evidenced by the absence of a C–H shoulder in the C 1s spectrum (bottom panel of Figure 1b). This provides evidence for full reversibility of the hydrogenation and the complete removal of hydrogen.

Calculations of the C 1s binding energies are indicated by vertical lines on the energy axis of Figure 1b and confirm the above assignment. The experimental and calculated C 1s peak positions for the constituents of the corresponding lineshapes are summarized in Table 1. For pristine graphene on Ni, our calculations yield C–Ni distances of 2.08 and 2.11 Å for top and hollow Ni sites, respectively, in good agreement to experiments.³⁸ The distance to the substrate increases to 3.15 Å for the weaker C–Au bonds which results in a significantly lowered cohesive energy of 6.60 eV/atom for C/Au³⁹ (C/Ni has 7.03 eV/atom). Figure 1c shows the optimized (8 × 8) on (9 × 9) geometry of the Au on Ni which we used for performing the calculations of the C 1s energies. We find the supercell has a length of 22.75 Å, which is in good agreement with previously reported values.^{28,40}

TABLE 1. Experimental and Theoretical C 1s Binding Energies for Graphene/Ni and Graphene/Au^a

	graphene/Ni		H-graphene/Au		
	top	hollow	C1	C2	C3
expt	284.7	284.8	284.2	283.9	284.7
calcd	284.80	284.89	284.33	283.59	284.61

^a For graphene/Ni, the carbon atoms are located above top and hollow Ni sites. If 1 ML of Au is intercalated between graphene and Ni, the binding energy of graphene is given by C1. The values C2 and C3 denote binding energies of extra peaks that appear upon hydrogenation and the formation of C–H bonds (see sketches in Figure 1a).

Figure 1d shows the NEXAFS spectra for pristine and hydrogenated graphene on Au from close to normal to close to grazing incidence. Here grazing incidence refers to the electric field vector normal to the sample surface. The NEXAFS spectra show two prominent features at 285.5 and 293 eV which correspond to the transitions from C 1s to the π^* and σ^* bands, respectively.⁴¹ The selection rules for the $1s \rightarrow 2p_z$ dipole transition imply a π^* intensity maximum

for grazing incidence. Similarly, the $1s \rightarrow 2p_{x,y}$ dipole transitions imply a σ^* maximum for normal incidence. For grazing incidence, the NEXAFS spectrum of pristine graphene is dominated by the π^* resonance. Indeed, this behavior is remarkably similar to the NEXAFS of graphite.¹⁹ Upon hydrogenation, we observe a strong decrease in the intensity of the π^* related peak. The attachment of atomic hydrogen to carbon atoms of graphene leads to the loss of π^* intensity and is explained by the reduced number of π -bonds due to the formation of sp^3 C–H bonds. For normal incidence (upper curves of Figure 1d), we observe an increase of intensity between 288 and 291 eV that can be identified as the energy position of the C–H^{*} resonance in hydrocarbons.⁴¹ These results nicely confirm the formation of C–H bonds which we also observe in XPS as discussed above (see Figure 1b). It is tempting to relate the loss of π^* intensity to an absolute H coverage. However, we find that a direct comparison is not as straightforward as in the case of the XPS because the NEXAFS spectrum is influenced by strong excitonic effects that shift the resonance peaks making the choice of the integration limits crucial.

Angle-Resolved Photoemission. We now turn to an analysis of the quasi-particle dispersion and a discussion of the electronic band structure of hydrogenated graphene. This is vital for unraveling changes close to E_F that determine optical and transport properties. To this end, we perform ARPES experiments, which is the most powerful technique to study electronic energy band dispersions and gives access to graphene's spectral function.⁴² A self-energy analysis allows us to estimate the hydrogen coverage independently from XPS and we find good agreement between the two methods.

Figure 2a shows the spectral function of graphene intercalated with Au in the ΓK direction. From the momentum dispersion of the π -band, we obtain a Fermi velocity of $v_F = 1.05 \times 10^6$ m/s, identical to that of graphite.⁴³ Interestingly, the third nearest neighbor (3NN) tight-binding (TB) calculations employing the previously reported TB parameters from graphite⁴⁴ yield a band structure that is fully consistent with the measured ARPES maxima of graphene on Au. Au intercalated graphene is therefore an ideal model system to study hydrogenation. Figure 2c displays the spectral function of graphene at the K point after in situ exposure to a beam of atomic hydrogen. Since the spectral function provides access to the imaginary part of the self-energy, $Im(\Sigma)$, we can estimate the increase in scattering time, τ , by using the Heisenberg uncertainty principle $Im(\Sigma)\tau \geq \hbar/2$, and therefore estimate the H concentration, η . To this end, we fitted constant energy cuts of the spectral function with Lorentzians in order to derive the momentum line widths Δk which are related to the imaginary part of the self-energy as $Im(\Sigma) = v_F \Delta k / 2$. With the mean free path of the electrons moving in 2D graphene given by $l = 1/\eta\lambda$, where λ is the linear scattering cross section of the H impurities, and $l = v_F\tau$, we find the scattering rate, valid for low H coverage, to be $f =$

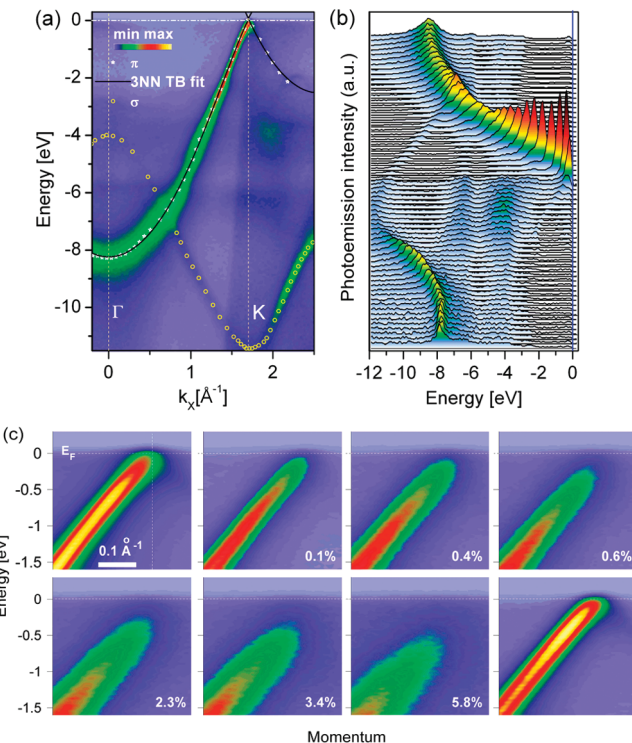


FIGURE 2. (a) ARPES spectrum of graphene/Au along with a 3NN TB calculation and (b) the raw photoemission data. (c) ARPES spectra around the K point of hydrogenated graphene with increasing H-coverage as denoted. The last image (bottom right) corresponds to graphene after thermal annealing.

$1/\tau = \eta v_F \lambda$. The cross section λ measures the linear dimension of the hydrogen impurity and is expected to be on the order of a few graphene lattice parameters. An estimate based on a simple tight-binding model of H adsorption on graphene is given by $1/\tau = (2\pi/\hbar)\eta A_c |t_0(\epsilon)|^2 \nu_0(\epsilon)$, where A_c is area per carbon atom, t_0 is a renormalized T -matrix element for scattering from a single impurity, ϵ is the electron energy, and ν_0 is the graphene electronic density of states per carbon atom.⁴⁵ Using the previously reported H–C TB parameters,⁴⁶ we found for a coverage of 6% ($\eta A_c = 0.06$) and an energy of 1 eV below Fermi level, $f = 1.0 \times 10^{15} \text{ s}^{-1}$, equivalent to a scattering cross section of $\lambda = 4.4 \text{ \AA}$. Therefore, the chemisorption of one hydrogen atom results in a lattice distortion felt by electrons inside a circle of radius 4.4 Å. This is in reasonable agreement with previous reported values.¹⁶ Notably, we do not include effects of inhomogeneous H clustering or the effect of varying chemisorption energies for an H atom that might lead to a different and not entirely random chemisorption pattern.

Turning back to Figure 2c, it is clear that already at low H/C ratios of 0.5%, we observe a dramatic decrease of the photoemission (PE) intensity of the π band close to E_F accompanied by a general broadening of the π -band. The most striking effect is the opening of a gap of reduced ARPES intensity between the π -band and E_F . The π band maxima are therefore not crossing E_F anymore but appear at lower

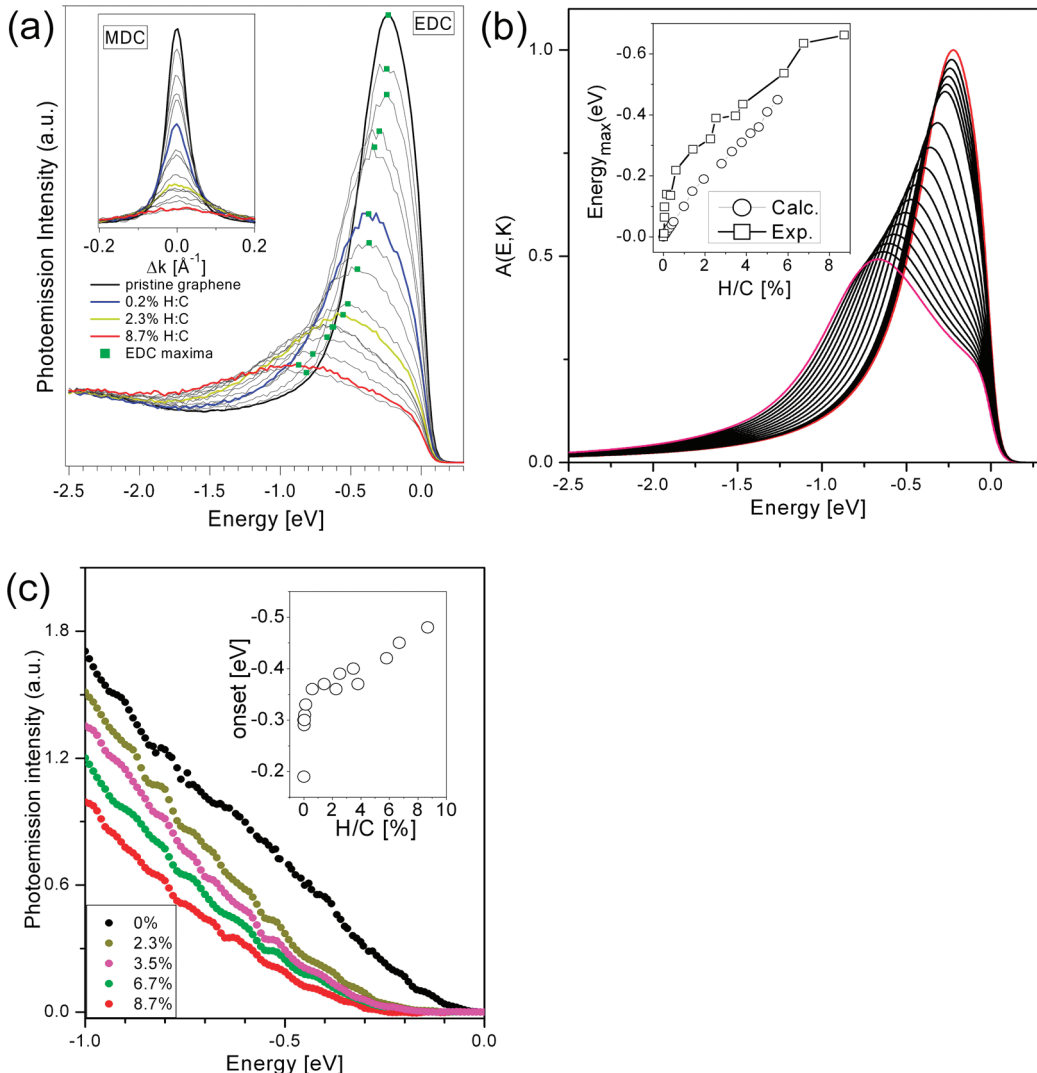


FIGURE 3. (a) Energy dispersion curves (EDC) and momentum dispersion curves (MDC) for 15 different hydrogenation stages as indicated. (b) Calculations of $A(E, K)$ for increasing hydrogen content between 0% and 5.5% (indicated by red color). The inset compares the calculated maxima of $A(E, K)$ to the experimental EDC maxima (relative shift to the curves for pristine graphene). (c) Angle-integrated PE intensity for different H/C ratios with the Au background intensity subtracted. The inset denotes the energy onset of the rise in intensity.

energies as hydrogenation proceeds. Finally, the last graph of Figure 2c shows the fully recovered π -band after annealing at 600 K, demonstrating the reversibility of this functionalization procedure. The energy dispersion curves (EDCs) through K (indicated by a vertical dashed line in the first viewgraph of Figure 2c) are displayed in Figure 3a. The EDCs have been integrated over 2° around K . It can be seen that the maxima of the EDCs shift by ~ 800 meV for 8.7% hydrogenation. As we will show later, this is directly related to a gap opening. The inset in Figure 3a depicts the momentum dispersion curves (MDCs) taken at 1 eV below E_F from which we determined the H/C ratio η as described above.

Several mechanisms responsible for the downshift of the π band are conceivable. First, the chemisorbed H might lead to graphene quantum dot formation and hence to size quantization resulting in the opening of a band gap. This effect might be especially important for a regularly chemi-

sorbed H superstructure. The strong increase in impurity scattering rate, however, points toward randomly chemisorbed H. Furthermore, assuming single sided attachment of H to graphene on a substrate, the lowest energy configurations for two neighboring H atoms break the sublattice symmetry.⁴⁷ Symmetry breaking in turn invariably leads to a gap opening which is proportional to the difference in potential energy felt by the hydrogenated and unhydrogenated carbon atoms. This would also explain the broadening of the spectral function $A(E, K)$: in this model there are sp^2 and sp^3 sites and the spectral weight is merely shifting between them. Clearly, other chemisorption patterns which do not break the sublattice symmetry are also conceivable but their contribution is much smaller as can be inferred from the agreement of the measured spectral functions and the model calculations for symmetry breaking H chemisorption sites as discussed below.

The cuts of the calculated spectral function $A(E, K)$ for single-sided hydrogenation are depicted in Figure 3b and are to be compared to the EDCs from Figure 3a. It can be seen that the shift of the maxima of $A(E, K)$ with proceeding hydrogenation, the broadening, and also the line shape are in good agreement to the experiments. The small remaining differences come from the fact that the experimental EDCs contain some intensity from the Au electronic states. Notably, we can only obtain the downshift of the maxima of $A(E, K)$ for our calculation if we impose the constraint that at most one C atom per graphene unit cell can be hydrogenated. This provides evidence that symmetry breaking is the mechanism responsible for the gap opening as seen in the ARPES spectra. The inset in Figure 3b compares the EDC maxima to the energy maximum of the calculated $A(E, K)$ and it is evident that they also agree well.

Looking at the downshift of the EDC maxima with hydrogenation, it is clear that this will also influence the total density of states (DOS) which is proportional to the angle integrated PE intensity. After performing the integration, we subtracted the small PE intensity of the underlying Au. The resulting integrated PE intensity of hydrogenated graphene for different η is depicted in Figure 3c. It is clear that for increasing η , the integrated PE intensity at a given energy is smaller which relates to the gap opening and puts our data in a wider context relevant for optical absorption experiments. This gap opening is also evident from the inset to Figure 3c where we depict the energy value at which the PE intensity starts to rise (we define this onset as 10% of the integrated PE intensity of pristine graphene at 1 eV). With proceeding hydrogenation, the onset energy appears at a lower energy, opening up a region of no PE intensity (i.e., a gap). Most importantly, this onset is directly related to half the band gap value since it is measured with respect to E_F if we assume electron–hole symmetry. In Figure 3c we have an onset energy of 0.5 eV for the maximum hydrogenation level. Therefore we expect twice this value, i.e., 1 eV for the electronic band gap between π and π^* . This is a perfect energy range for optical applications, and it is also in agreement with calculated values.^{22,48}

Discussion and Conclusions. In summary we have investigated the functionalization of quasi-free-standing graphene with atomic hydrogen. The XPS measurements of graphene have shown a C 1s core level shift of 0.5 eV toward lower binding energy upon Au intercalation in between the graphene/Ni(111) interface, resulting in a substantial reduction of the substrate interaction. This is in accordance with our calculations that predict a reduction of the cohesive energy per atom by 0.4 eV and an increase of the graphene–substrate distance by 1 Å. The exposure of graphene to atomic hydrogen induces the formation of C–H bonds resulting in a local sp^3 hybridization. This is directly observed in XPS by the appearance of two additional C 1s peaks originating from the C–H bond and the C atom next to it. These two features are separated by almost 1 eV from each

other, which is also in good agreement with the C 1s binding energy calculations (see the features C2 and C3 depicted in Figure 1b). NEXAFS measurements indicate a rehybridization from sp^2 to sp^3 and the formation of C–H bonds perpendicular to the graphene layer. Most importantly, the ARPES spectra of hydrogenated graphene clearly show the downshift of the π band's spectral function to lower energies and also a broadening. Our calculations support sublattice symmetry breaking as the reason for the observed changes in the ARPES upon hydrogenation. Since the energy difference between the onset of the integrated PE intensity (proportional to the DOS) and E_F is related to half the electronic band gap value, we expect tunable optical properties for hydrogenated graphene. Our results also unraveled an interesting connection between the hydrogenation of graphene and amorphous carbon. On the one hand, the origin for the tunable optical band gap in a-C:H¹⁹ might also be understood in terms of sublattice symmetry breaking. On the other hand, hydrogenation might as well also lead to functional optical devices based on graphene because the electronic band gap can be tuned with hydrogen coverage. Our results are therefore also relevant to optical absorption, photoluminescence, and resonance Raman spectroscopy of graphene. First, the optical gap should be observable and possibly lead to photoluminescence, similar to the case of oxidized graphene.⁴⁹ The broad peak maximum in the spectral function would manifest itself as the so-called Urbach tails in the optical absorption spectrum, similar to the case of a-C:H. Second, it is well-known that hydrogenated graphene shows an increase in its D band Raman spectrum which is due to the randomly chemisorbed H atoms that act as defects.²³ Little is known about the relation of the D band intensity to the absolute number of defects. We therefore propose a combined photoemission and resonance Raman study of hydrogenated graphene with a defined H coverage to determine the relation between D band Raman intensity and H/C ratio. Such a defined environment is extremely important for a quantitative understanding of the defect scattering-induced D band and also for the emerging field of graphene metrology.

Acknowledgment. D.V. acknowledges DFG Grant No. VY 64/1-1. S.T. and S.S. acknowledge CINECA Consortium (Bologna, Italy) for providing technical support and access to high-performance supercomputers and Drs. Lucia Calliari and Giorgio Speranza for useful discussions. B.D. was supported by the Hungarian Scientific Research Fund No. K72613 and CNK80991 and by the Bolyai program of the Hungarian Academy of Sciences. M.F. acknowledges funding from the Iranian Nanotechnology Initiative. T.P. acknowledges project FWF-I377-N16. M.S.D. acknowledges support from NSF-DMR 07-04197. A.G. and M.K. acknowledge DFG Grant No. GR 3708/1-1. A.G. further acknowledges an APART fellowship from the Austrian Academy of Sciences, a Marie Curie Reintegration grant (ECO-GRAPHENE), and EU support through ELISA for the stay at BESSY.

Supporting Information Available. Details on calculation of core level binding energies, DFT calculations, and spectral function calculations. This material is available free of charge via the Internet at <http://pubs.acs.org>.

REFERENCES AND NOTES

- (1) Novoselov, K. S.; Geim, A. K.; Morozov, S. V.; Jiang, D.; Zhang, Y.; Dubonos, S. V.; Grigorieva, I. V.; Firsov, A. A. *Science* **2004**, *306*, 666–669.
- (2) Geim, A. K.; Novoselov, K. S. *Nat. Mater.* **2007**, *6*, 183–191.
- (3) Katsnelson, M. I.; Novoselov, K. S.; Geim, A. K. *Nat. Phys.* **2006**, *2*, 620–625.
- (4) Castro-Neto, A. H.; Guinea, F.; Peres, N. M. R.; Novoselov, K. S.; Geim, A. K. *Rev. Mod. Phys.* **2009**, *81*, 109.
- (5) Han, M. Y.; Ozilmez, B.; Zhang, Y.; Kim, P. *Phys. Rev. Lett.* **2007**, *98*, 206805.
- (6) Li, X.; Wang, X.; Zhang, L.; Lee, S.; Dai, H. *Science* **2008**, *319*, 1229–1232.
- (7) Taioli, S.; Umari, P.; Souza, M. M. D. *Phys. Status Solidi B* **2009**, *246*, 2572–2576.
- (8) Saito, R.; Dresselhaus, G.; Dresselhaus, M. S. *Physical Properties of Carbon Nanotubes*; Imperial College Press: London, 1998.
- (9) Stampfer, C.; Schurtenberger, E.; Molitor, F.; Guttinger, J.; Ihn, T.; Ensslin, K. *Nano Lett.* **2008**, *8*, 2378–2383.
- (10) Son, Y.-W.; Cohen, M. L.; Louie, S. G. *Phys. Rev. Lett.* **2006**, *97*, 216803.
- (11) Schedin, F.; Geim, A. K.; Morozov, S. V.; Hill, E. W.; Blake, P.; Katsnelson, M. I.; Novoselov, K. S. *Nat. Mater.* **2007**, *6*, 652–655.
- (12) Gierz, I.; Riedl, C.; Starke, U.; Ast, C. R.; Kern, K. *Nano Lett.* **2008**, *8*, 4603–4607.
- (13) Ryu, S.; Han, M. Y.; Maultzsch, J.; Heinz, T. F.; Kim, P.; Steigerwald, M. L.; Brus, L. E. *Nano Lett.* **2008**, *8*, 4597–4602.
- (14) Farjam, M.; Rafii-Tabar, H. *Phys. Rev. B* **2009**, *79*, No. 045417.
- (15) Wehling, T. O.; Katsnelson, M. I.; Lichtenstein, A. I. *Phys. Rev. B* **2009**, *80*, No. 085428.
- (16) Boukhalov, D. W.; Katsnelson, M. I. *J. Phys.: Condens. Matter* **2009**, *21*, 344205.
- (17) Robertson, J.; O'Reilly, E. P. *Phys. Rev. B* **1987**, *35*, 2946–2957.
- (18) Fink, J.; Müller-Heinzerling, T.; Pflüger, J.; Scheerer, B.; Dischler, B.; Koidl, P.; Bubenzier, A.; Sah, R. E. *Phys. Rev. B* **1984**, *30*, 4713–4718.
- (19) Fink, J.; Müller-Heinzerling, T.; Pflüger, J.; Bubenzier, A.; Koidl, P.; Crecelius, G. *Solid State Commun.* **1983**, *47*, 687–691.
- (20) Sofo, J. O.; Chaudhari, A. S.; Barber, G. D. *Phys. Rev. B* **2007**, *75*, 153401.
- (21) Savini, G.; Ferrari, A. C.; Giustino, F. ArXiv e-prints, 2010.
- (22) Duplock, E. J.; Scheffler, M.; Lindan, P. J. D. *Phys. Rev. Lett.* **2004**, *92*, 225502.
- (23) Elias, D. C.; Nair, R. R.; Mohiuddin, T. M. G.; Morozov, S. V.; Blake, P.; Halsall, M. P.; Ferrari, A. C.; Boukhalov, D. W.; Katsnelson, M. I.; Geim, A. K.; Novoselov, K. S. *Science* **2009**, *323*, 610–613.
- (24) Bostwick, A.; McChesney, J. L.; Emtsev, K. V.; Seyller, T.; Horn, K.; Kavan, S. D.; Rotenberg, E. *Phys. Rev. Lett.* **2009**, *103*, No. 056404.
- (25) Balog, R.; et al. *Nat. Mater.* **2010**, *9*, 315–319.
- (26) Grüneis, A.; Kummer, K.; Vyalikh, D. V. *New J. Phys.* **2009**, *11*, 073050.
- (27) Preobrajenski, A. B.; Ng, M. L.; Vinogradov, A. S.; Martensson, N. *Phys. Rev. B* **2008**, *78*, No. 073401.
- (28) Varykhalov, A.; Sanchez-Barriga, J.; Shikin, A. M.; Biswas, C.; Vesco, E.; Rybkina, A.; Marchenko, D.; Rader, O. *Phys. Rev. Lett.* **2008**, *101*, 157601.
- (29) Taioli, S.; Simonucci, S.; Dapor, M. *Comput. Sci. Discovery* **2009**, *2*, 015002.
- (30) Taioli, S.; Simonucci, S.; Calliari, L.; Filippi, M.; Dapor, M. *Phys. Rev. B* **2009**, *79*, No. 085432.
- (31) Ziegler, K.; Dóra, B.; Thalmeier, P. *Phys. Rev. B* **2009**, *79*, 235431.
- (32) Ziegler, K. *Phys. Rev. Lett.* **2009**, *102*, 126802.
- (33) Dóra, B.; Ziegler, K. *New J. Phys.* **2009**, *11*, No. 095006.
- (34) Doniach, S.; Sunjic, M. J. *Phys. C: Solid State Phys.* **1970**, *3*, 285.
- (35) Nikitin, A.; Ogasawara, H.; Mann, D.; Denecke, R.; Zhang, Z.; Dai, H.; Cho, K.; Nilsson, A. *Phys. Rev. Lett.* **2005**, *95*, 225507.
- (36) Nikitin, A.; Näslund, L.-A.; Zhang, Z.; Nilsson, A. *Surf. Sci.* **2008**, *602*, 2575–2580.
- (37) Wessely, O.; Katsnelson, M. I.; Nilsson, A.; Nikitin, A.; Ogasawara, H.; Odelius, M.; Sanyal, B.; Eriksson, O. *Phys. Rev. B* **2007**, *76*, 161402.
- (38) Gamo, Y.; A. N.; Wakabayashi, M.; Oshima, C. *Surf. Sci.* **1997**, *374*, 61.
- (39) The cohesive energy in an inhomogenous material is given by the difference of the bulk total energy of the compound solid and the total energy of free atoms of different species, weighted by the number of atoms of each species, divided by the total number of atoms itself.
- (40) Jones, T.; Noakes, T.; Bailey, P.; Baddeley, C. *Surf. Sci.* **2006**, *600*, 2129–2137.
- (41) Stöhr, J. *NEXAFS Spectroscopy*; Springer-Verlag: Berlin, 1996.
- (42) Hüfner, S. In *Photoelectron spectroscopy*; Springer-Verlag: Berlin, 1996.
- (43) Grüneis, A.; Attaccalite, C.; Pichler, T.; Zabolotnyy, V.; Shiozawa, H.; Molodtsov, S.; Inosov, D.; Koitzsch, A.; Knupfer, M.; Schiessling, J.; Follath, R.; Weber, R.; Rudolf, P.; Wirtz, L.; Rubio, A. *Phys. Rev. Lett.* **2008**, *100*, No. 037601.
- (44) Grüneis, A.; Attaccalite, C.; Wirtz, L.; Shiozawa, H.; Saito, R.; Pichler, T.; Rubio, A. *Phys. Rev. B* **2008**, *78*, 205425.
- (45) Robinson, J. P.; Schomerus, H.; Oroszlány, L.; Falko, V. I. *Phys. Rev. Lett.* **2008**, *101*, 196803.
- (46) Vergés, J. A.; de Andres, P. L. *Phys. Rev. B* **2010**, *81*, No. 075423.
- (47) Boukhalov, D. W.; Katsnelson, M. I.; Lichtenstein, A. I. *Phys. Rev. B* **2008**, *77*, No. 035427.
- (48) Casolo, S.; Lovvik, O. M.; Martinazzo, R.; Tantardini, G. F. *J. Chem. Phys.* **2009**, *130*, No. 054704.
- (49) Gokus, T.; Nair, R. R.; Bonetti, A.; Bohmeler, M.; Lombardo, A.; Novoselov, K. S.; Geim, A. K.; Ferrari, A. C.; Hartschuh, A. *ACS Nano* **2009**, *3*, 3963–3968.